Available online at https://link.springer.com/journal/42241
http://www.jhydrodynamics.com
Journal of Hydrodynamics, 2022, 34(2): 226-233
https://doi.org/10.1007/s42241-022-0021-8

Vortex structures of dynamic pure yaw test using DDES approach and vortex identification method

Wei-wen Zhao[1], Qing-jie Meng[2], De-cheng Wan[1*], Yi-qian Wang[3]
1. *Computational Marine Hydrodynamics Lab (CMHL), School of Naval Architecture, Ocean and Civil Engineering, Shanghai Jiao Tong University, Shanghai 200240, China*
2. *Wuhan Second Ship Design and Research Institute, Wuhan 430205, China*
3. *School of Mathematical Science, Soochow University, Suzhou 215006, China*

(Received November 23, 2021, Revised February 25, 2022, Accepted February 26, 2022, Published online April 19, 2022)

Abstract: Considered as the building blocks, vortex structures with variety of sizes and intensity are widely recognized in the viscous flow field around ship. In this paper, the computational fluid dynamics (CFD) solver, naoe-FOAM-SJTU, coupled with delayed detached-eddy simulation (DDES) is adopted to analyze the vortex structures around the benchmark model Yupeng ship in dynamic pure yaw tests, which are captured by third generation of vortex identification method. The good agreement of the predicted force/moment by DDES method with the experimental data indicates that the present numerical schemes are reliable and robust. Three vortex identification methods, Q-criteria, Ω_R and Liutex, are used to capture the vortex structures around the hull. The large separated flow is able to be investigated by these three methods, in which more vortex structures are captured by Ω_R approach and Liutex method with scalar, vector and tensor form seems to be more suitable for analyzing the flow mechanism around the hull in dynamic pure yaw test. In general, each vortex structure corresponds to a dominant positive/negative axial Liutex and a bound vortex pair. The streamlines are spiral in the large separated flow, indicating that the flow in corresponding region is rotational. But the rotation of the flow is not directly related to the intensity of Liutex.

Key words: Dynamic pure yaw test, delayed detached-eddy simulation (DDES), vortex identification method, vortex structure, flow mechanism

Introduction

Considered as the tendon of turbulence, vortex plays a critical role in the negation, evolution and mechanism of turbulence. There are a large number of vortex structures around the hull, which can be used to study the flow mechanism around the hull. To explore the flow mechanism in the ship flow field, extensive studies have been conducted worldwide by experiments and computational fluid dynamics (CFD). As a typical hydrodynamic experiment including static drift test, dynamic pure sway and pure yaw tests, ship planar motion mechanism (PMM) is not only used to predict the hydrodynamic derivatives of ships, but also to analyze the flow mechanism in the large separated flow of ships. In addition, CFD is rapidly becoming increasingly popular on the ship hydrodynamics. The researchers in the University of Iowa have developed the unsteady Reynold-averaged Naiver-Stokes (URANS) solver, CFDShip-Iowa, based on finite difference method (FDM). The CFD solver naoe-FOAM-SJTU, based on the open-source code platform OpenFOAM, is also developed by the Computational Marine Hydrodynamic Labs (CMHL) in Shanghai Jiao Tong University. These CFD solvers have been widely applied in ocean engineering.

In 2005, Simonsen and Stern[1] used the solver, CFDShip-Iowa, to simulate the flow field of the appended Esso Osaka ship. It was found that the vorticity on the both sides of the hull is asymmetric and the vortex structures induced by the bilge keel

Project supported by the National Natural Science Foundation of China (Grant Nos. 51909160, 51879159 and 52131102), the National Key Research and Development Program of China (Grant No. 2019YFB1704200).
Biography: Wei-wen Zhao (1990-), Male, Ph. D.,
E-mail: weiwen.zhao@sjtu.edu.cn
Corresponding author: De-cheng Wan,
E-mail: dcwan@sjtu.edu.cn

was visible in the static drift tests. Xing et al.[2-4] analyzed the capability of the blended $k\text{-}\varepsilon / k\text{-}\omega$ (BKW) RANS models and BKW-detached-eddy simulation (DES) to simulate the viscous flow field of KVLCC2 at drift angle 0°, 12°, 30° and 60°. In the study, a Karman-like vortex shedding was found in the flow field. Ohashi and Hino[5] compared the complex flow structures behind a cylinder wall, which were calculated by RANS, DES and delayed detached-eddy simulation (DDES) methods. The results proved the validity of DES and DDES for simulating the large separated flows. Wang et al.[6], Ren et al.[7] simulated the bow wave breaking of KRISO Container Ship (KCS) by DDES and RANS methods. It was found that DDES approach was able to capture more scars and plunging wave breaking, indicating that DDES approach was more suitable for simulating the fine flow field around the hull.

In the numerical simulations, vortex structures were usually used to analyze the flow mechanisms in the viscous flow field. Kandasamy et al.[8], Xing et al.[9] analyzed the instability mechanisms of unsteady free surface around a foil NACA0024, which was penetrating the free surface. By comparing with the results presented in the experiments and calculated by DES, they found that large-scale unsteady vortex structures could be well captured by DES and RANS approaches. But the vortices were rapidly dissipated by RANS downstream. Pinto-Heredero et al.[10] used the CFD solver, CFDShip-Iowa, to calculate the viscous flow field around the Wigley hull at drift angle between 10° and 60°. Their study indicated that there was a significant relationship between the vortex structures and Kelvin wave pattern on the free surface. Bhushan et al.[11] performed the numerical simulations of appended Athena in full scale conditions by DES method. The dominant frequency of transom flow was explained by vortical structures and associated instabilities. Heydari and Sadat-Hosseini[12] studied the vortex structures around a propeller in the viscous flow field.

Sakamoto et al.[13-14], Yoon et al.[15-16] simulated the static and dynamic PMM tests of DTMB5415. The hydrodynamic derivatives related to the ship maneuverability are predicted and compared with the experimental results. In addition, the viscous flow field was also analyzed in details, including the wave generation on the free surface and the vorticity field around the hull. The hydrodynamic variations were explained by the change of local flow field. Meng and Wan[17] carried out the numerical simulations for static drift tests of KVLCC2M in deep and shallow water, respectively. The settlement effect of the hull in shallow water was obtained. Ren et al.[18] used the third generation of vortex identification method to capture the vortex structures in the viscous flow field solved by RANS method. The time histories of force and moment were in good agreement with the experiment.

So far, PMM tests are used to predict the hydrodynamic derivatives of ships. The flow mechanism in the dynamic pure yaw tests is rarely analyzed, especially by the third generation of vortex identification methods. While, this paper will display more details in the viscous flow field of dynamic pure yaw tests for Yupeng ship.

In the present work, the authors simulate the dynamic pure yaw test by DDES methods. The CFD solver, naoe-FOAM-SJTU, is the self-developed one based on open-source code platform OpenFOAM. Next is the framework of this paper. The first part is the basic numerical approach. The second part is the geometry model of Yupeng ship, test conditions and grid generation in numerical calculation. The results show the force and moment, free surface, vortex structures, axial Liutex and streamline and flow field. Finally, the conclusion of this paper is drawn.

1. Numerical approach

The in-house CFD solver naoe-FOAM-SJTU[19-21] is adopted in the presented numerical calculation. For viscous flow field, the governing equations are solved and the governing equations contain a mass conservation equation and a moment conservation equation. The free surface is captured by a high-resolution VOF method in which the bounded compression technique[22] is applied. The two-equation model, shear stress transport (SST) $k\text{-}\omega$ model, is used to solve Reynold stress. The transport equations[6] of the turbulent kinetic energy k and the specific dissipation ω are given by:

$$\frac{\partial k}{\partial t}+\nabla\cdot(Uk)=\tilde{G}-\beta^{*}k\omega+\nabla\cdot[(\nu+\sigma_{k}\nu_{t})\nabla k] \tag{1}$$

$$\frac{\partial \omega}{\partial t}+\nabla\cdot(U\omega)=\gamma S^{2}-\beta\omega^{2}+\nabla\cdot[(\nu+\sigma_{\omega}\nu_{t})\nabla\omega]+(1-F_{1})CD_{k\omega} \tag{2}$$

where the blending function F_1 is used to combine the $k\text{-}\varepsilon$, $k\text{-}\omega$ model. More details of SST $k\text{-}\omega$ model can be found in literature[23].

As for the DDES method, it is the modification of DES method by redefining the turbulent length scale, l_{DDES}, which is able to avoid the RANS calculation area being switched to large eddy simulation (LES) mode too early.

$$l_{\mathrm{DDES}}=l_{\mathrm{RANS}}-f_{d}\max(0,l_{\mathrm{RANS}}-C_{\mathrm{DES}}\Delta) \tag{3}$$

where f_d is the empirical blending function defined

as:

$$f_d = 1 - \tanh\left[\left(C_{d1} r_d\right)^{C_{d2}}\right] \tag{4}$$

$$r_d = \frac{\nu_t + \nu}{\kappa^2 d_w^2 \sqrt{0.5(S^2 + \Omega^2)}} \tag{5}$$

where ν_t is the eddy viscosity, ν represents the molecular viscosity, κ is the von Karman constant and d_w is the distance to wall. The implementation of the DDES approach in the naoe-FOAM-SJTU solver can be referred in the literature[24-25].

In the present numerical calculation, the dynamic overset grid technology[19] is applied for the large amplitude motion in the dynamic pure yaw tests. To accurately present the details in the viscous flow field, the third generation of vortex identification methods are applied in the numerical simulations. The results obtained by Ω_R and Liutex (third generation) are compared with the vortex structures by Q - criteria (second generation). Related theory of the third generation is referred to literature[26].

2. Numerical simulation setup

2.1 *Geometry model*

The ship model, Yupeng ship, was selected as significant ships by The Royal Institution of Naval Architects in 2016. Its L_{pp} is 3.857m with 0.21 m draft. Its principal particulars and geometry are presented in Table 1, Fig. 1. In the present study, the scale ratio of the ship is 49. Extensive experiments are performed in the towing tank of Marine design and Research Institute of China (MARIC). In the experiments and the present study, the speed is 1.323 m/s with heave and pitch being taken into consideration. The amplitude of swaying motion is 0.4 m with the period being 8 s. The reference point of forces and moments is the center of gravity, as shown in Fig. 2.

Table 1 Principal particulars of Yupeng Ship

Main particulars	Value
Length between perpendiculars, L_{pp} /m	3.857
Beam, B_{WZ} /m	0.567
Draft, T_M /m	0.210
Block coefficient, CB /m	0.721
Longitudinal inertial radius, R_{yy} /m	0.984

Fig. 1 (Color online) Geometry model of Yupeng Ship

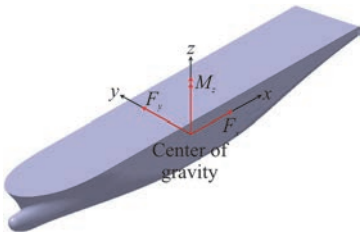

Fig. 2 (Color online) Coordinate system of force and moment

2.2 *Grid generation*

Figure 3 presents the computational domain and boundary conditions in the current simulation. The commercial software, HEXPRESS, is applied for the grid generation referred the literature[18], in which the mesh independence is also completed. For capturing the local fine viscous flow field, a block is adopted to refine the grid near the overlap domain which contains the hull and the grid near free surface is also refined. The total grid number slightly increased for applicating DDES method more reasonably and reached about 8.36 million. The grid distribution is shown in Fig. 4. The red lines represent the background grid distribution and the blue is the hull in Fig. 4 (a). Figure 4 (b) displays the grid distribution on the hull.

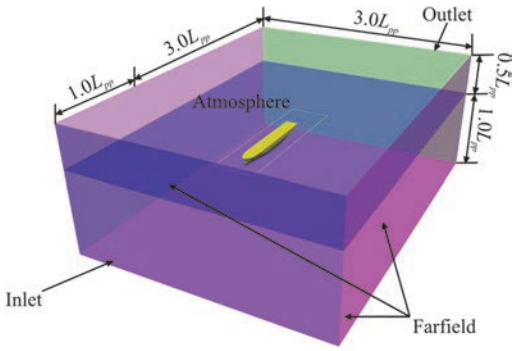

Fig. 3 (Color online) Computational domain

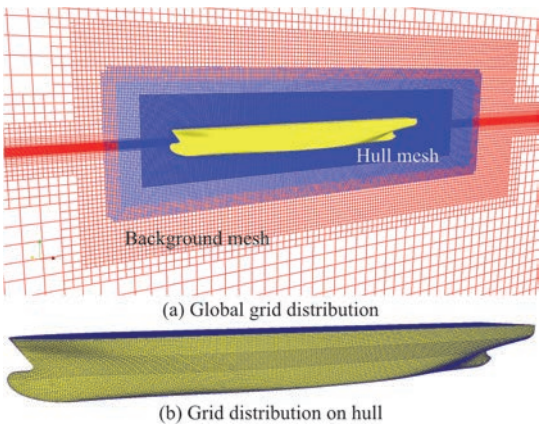

Fig. 4 (Color online) Grid distribution

3. Results and discussion

3.1 *Force and moments*

Since the dynamic pure yaw test is the superposition of static drift test and dynamic pure sway test, the hydrodynamic performance and viscous flow field are more difficult to predict accurately. To evaluate the errors of force and moment, the mean value of the time histories is used for resistance, and the amplitudes of their time histories are adopted for the lateral force and yawing moment.

Figure 5, Table 2 show the comparison between force and moment obtained by DDES and experiment. The resistance is obviously periodical in the dynamic pure yaw motion. This is mainly due to the periodic variation of the yaw angle. In terms of the lateral force and yawing moment, the predicted results are in good agreement with experimental data. Table 2 lists the errors of force and moment in the dynamic pure yaw test. The yawing moment is more accurately predicted than resistance and lateral force. The lateral force is under-estimated by 15% in both numerical simulations. While the resistance is over-predicted by 14%. The predicted results are acceptable.

3.2 *Vortex structure*

Figure 6 presents the vortex structures in the dynamic pure yaw test. Overall, more complex vortex structures are captured by Ω_R method. Not only the dominant vortex structures but also the bound ones are captured by this method, since it represents the relative strength. It is also found that large sheet vortex structures occur near the bow on the free surface. In addition, a long vortex structure originating from the propeller shaft is also captured by these three methods.

At T, a vortex structure originating from the bulb on the starboard sheds off from the shoulder of the hull and is broken after contacting the hull again downstream. Since the hull yaw from starboard to portside at this time, it was difficult for this vortex structure to develop in the far field. At $T+1/4T$, the yaw angle reaches the maximum. A vortex structure originates from the bilge on the portside, shedding from the hull approximately at the middle of the hull, and then rapidly splitting into a strong main vortex structure and a weak vortex pair. This phenomenon will be further analyzed in the next. The vortex structures at $T+1/2T$, $T+3/4T$ are the mirror of vortex structures at T, $T+1/4T$, respectively.

3.3 *Axial Liutex and streamline*

There are two significant times in the dynamic pure yaw test. One is the time T when the yaw angular velocity reaches maximum with yaw angle being zero. At $T+1/4T$, the yaw angular velocity is zero with yaw angle being maximum. Figures 7, 8 present the vortex structures based on Liutex method and the axial Liutex and streamlines at T, respectively. Figures 9, 10 depict the results at $T+1/4T$.

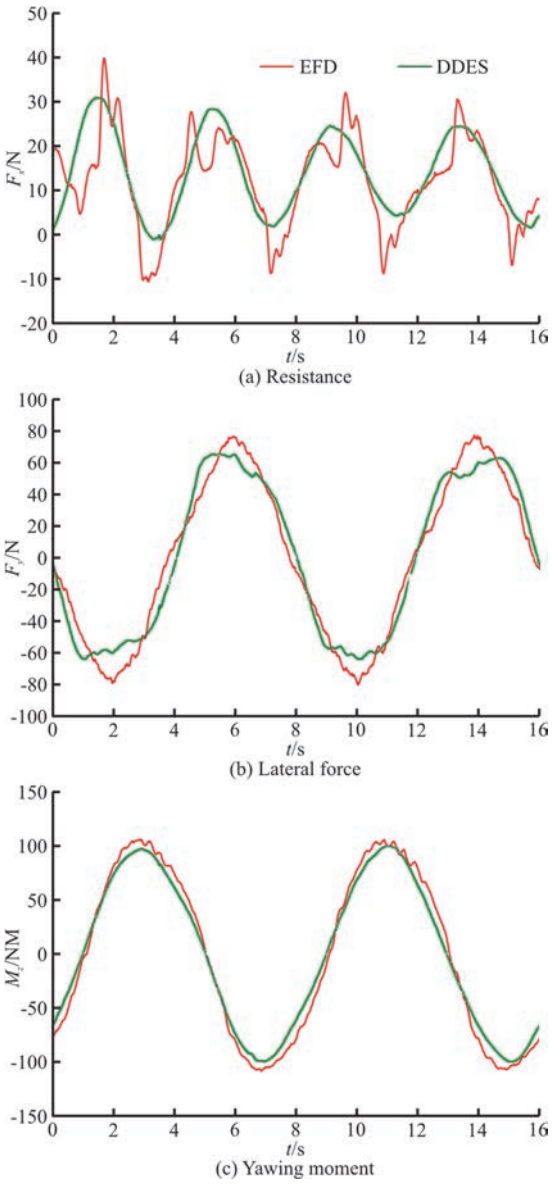

Fig. 5 (Color online) Time histories of forces and moment

Table 2 Comparison between predicted and experimental forces and moment in pure yaw tests

Force/moment	EFD	DDES	Error
Resistance/N	12.75	13.99	14.24%
Lateral force/N	77.78	65.67	–15.57%
Yawing moment/NM	106.95	100.47	–6.06%

Figure 7 shows the evolution of vortex structures around the hull at T. There are three dominant integral vortex structures investigated in the Fig. 7(a),

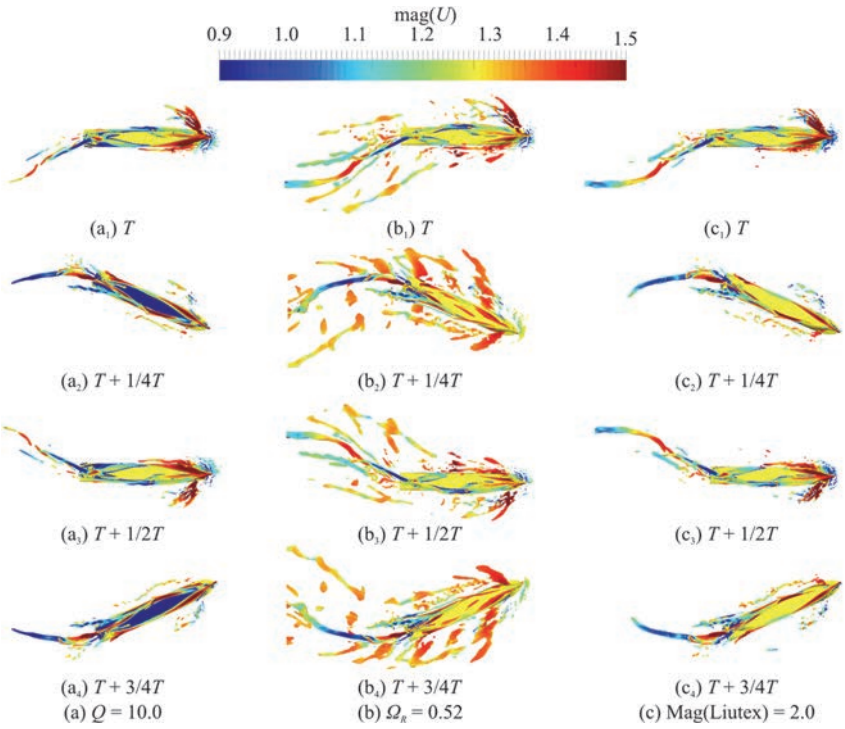

Fig. 6 (Color online) Vortex structure obtained by different vortex identification method

which consist of bow bilge vortex, stern vortex and shoulder vortex, and two bound breaking vortex structures such as bow wave vortex and fractional vortex. The bow bilge vortex structures including a dominant vortex and a bound vortex originate from the bilge of bulb bow, which are shown in Fig. 7(b) and marked as 1, 2 and 3, and gradually weak downstream. At last, the dominant vortex goes to merge with the stern vortex. Another dominant vortex, shoulder vortex structures, are deriving from the bow near the free surface on the portside. Near the stern, the stern vortex structures start from the propeller shaft and consist of three vortex structures which are labeled as S.V.1, S.V.2 and S.V.3, as depicted in Fig. 7(c). Since the evolution of bow wave, the bow wave vortex structures are captured on the starboard. In addition, there are much fractional vortex structures near the bow on the portside.

Figure 8 presents the axial Liutex and streamlines passing through the main vortex structures at T when the yawing angular velocity is maximum. Figure 8(a) shows the evolution of the main vortex structures and streamlines from global perspective. It is found that the dominant positive/negative axial Liutex and a bound vortex pair are corresponding to the vortex structures investigated in Fig. 7(a). The positive Liutex 1 (P.L.1) and vortex pair (V.P.1) originate from the bilge of the bulb and gradually disappears at the stern. The vortex pair (V.P.1) merges with the positive Liutex (P.L.1) near the mid-hull. The streamline 1 (S.L.1) corresponds well to the position where the strong axial Liutex concentrates and it is spiral. However, the pitch of S.L.1 before the shoulder is very large, as shown in Fig. 8(b), but decreases rapidly after crossing the shoulder, indicating that the axial Liutex increases behind the shoulder. The streamline 2 (S.L.2) develops downstream along the bottom of the hull, as depicted in Fig. 8(b). In the wake field, there is a dominant negative Liutex (N.L.2.0), corresponding to the stern vortex. Expect the dominant negative Liutex, there are one positive (P.L.2.1) and one negative axial Liutex (N.L.2.2), which are visible in Fig. 8(c). On the portside, the dominant positive Liutex (P.L.3) occurs near free surface, where the streamlines (S.L.3) pass through the vortex structures. In addition, there are two vortex pairs (V.P.4, V.P.5) on the starboard. The V.P.4 is corresponding to a fine vortex structure depicted in Fig. 7(b). The V.P.5 is the axial Liutex near the bow wave on the starboard.

Figure 9 shows the evolution of vortex structures around the hull when the yaw angle is maximum. Three significant vortex structures, bilge vortex, stern vortex and bow wave vortex, are captured by Liutex method, as shown in Fig. 9(a). There is also one fractional vortex structures near the bow wave on the starboard. The bilge vortex structures originate from the shoulder of the hull and are decomposed into four vortex structures downstream, marked as B.V.1 to B.V.4., as presented in Fig. 9(b). The decomposition of vortex structures indicates that the large separated flow occurs near the mid-hull. And the tail of B.V.1 is

spiral. Other significant vortex structures, stern vortex structures, are deriving from the propeller shaft. Bound vortex structures are captured near the dominant stern vortex structures in the wake field, which are visible in Figs. 9(a), 9(c). The last obvious vortex structures, bow wave vortex structures, are the spiral, as shown in Figs. 9(a), 9(b). In addition, the fractional vortex structures are captured near the bow wave on the starboard, which are induced by the bow wave breaking and overturning.

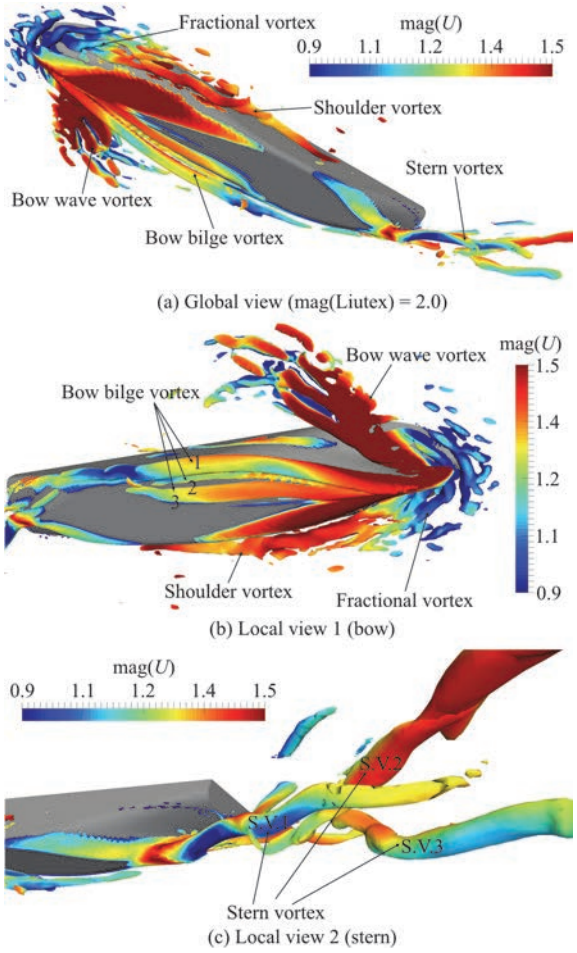

Fig. 7 (Color online) Vortex structure at T (mag(Liutex) = 2.0)

Figure 10 displays the evolution of axial Liutex and streamline at $T+1/4T$ when the yaw angle is maximum and the lateral velocity points to the portside from the starboard with the maximum. At this time, the main vortex structures mainly concentrate on the portside of the hull. In the global view, there are one significant positive axial Liutex which originates from the bilge near the mid-hull and one important negative Liutex deriving from the propeller shaft. A vortex pair 1 (V.P.1) is investigated at the bow bilge of the hull. The vortex pair 1 is decomposed into two vortex pair (V.P.1.1, V.P.1.2), which are shown in Figs. 10(a), 10(b). At this time, the large separated flow occurs near the bilge at the mid-hull since the yaw angle is maximum, as a result the flow passes through from the starboard to the portside of the hull. The flow is indicated by the streamline 1 (S.L.1). The positive Liutex (P.L.4) is corresponding to the bow wave vortex, as shown in Figs. 10(a), 10(b) and Figs. 9(a), 9(b). Figure 10(c) depicts the axial Liutex and streamlines in the wake field. It is found that the negative Liutex 2 (N.L.2) is dominant in the flow field and a bound positive Liutex (P.L.2) is also able to captured. In addition, the streamlines are spiral, indicating that the fluid in the wake field is rotational.

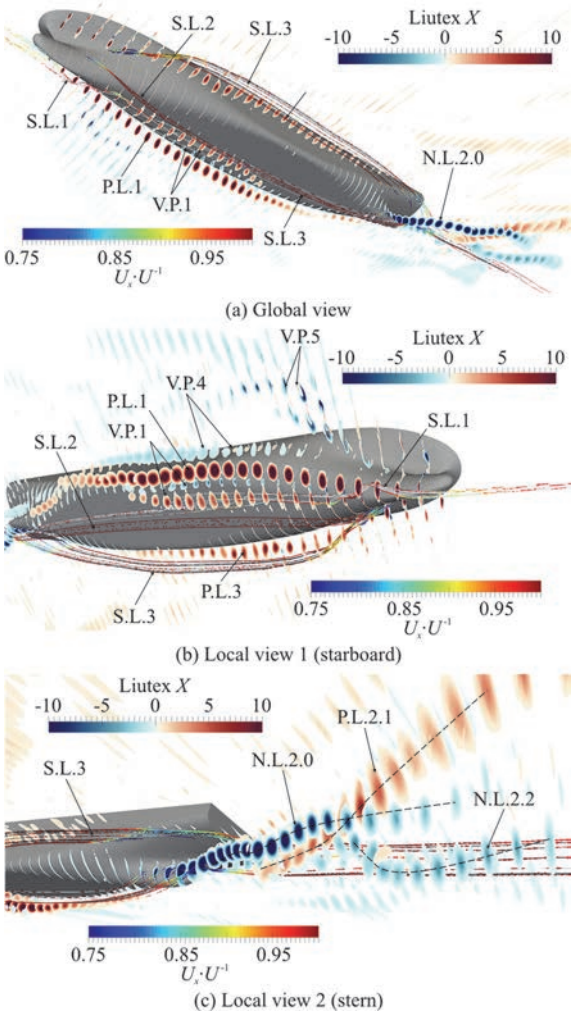

Fig. 8 (Color online) Evolution of axial Liutex and streamlines at T

4. Conclusions

In this paper, the CFD solver naoe-FOAM-SJTU that is self-developed based on the open-source code platform, OpenFOAM, is adopted to simulate the dynamic pure yaw tests of Yupeng ship. The viscous

flow field is solved by DDES approach coupling with dynamic overset grid technology. Not only the hydrodynamic performance is analyzed but also the flow mechanism in the viscous flow field is presented by three vortex identification methods and streamline.

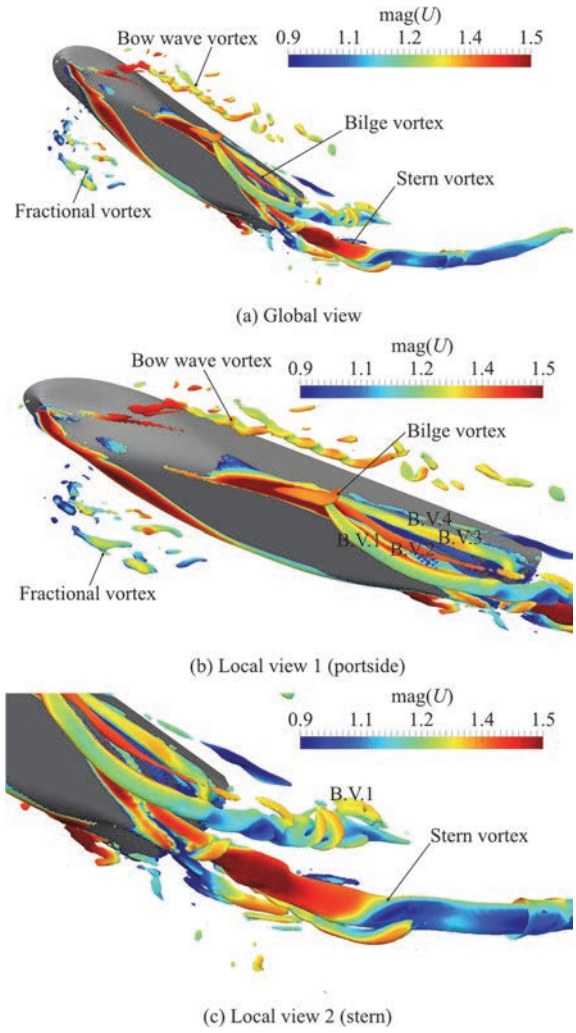

Fig. 9 (Color online) Vortex structure at $T+1/4T$ (mag(Liutex) = 2.0)

As for the hydrodynamic performance, the predicted forces and moment obtained by DDES methods are in good agreement with the experimental data. Although there is big fluctuation of the resistance in the experiment, the error of resistance is acceptable in the current simulations. The time histories of force and moment are compared with the experimental data, and the force and moment are accurately predicted.

By analyzing the vortex structures and streamlines in the flow field solved by DDES approach, it is found that DDES method is very suitable for simulating the large separated flow around the hull. The yaw motion induces the intense turbulent flow in the dynamic pure yaw tests. By analyzing the vortex structures obtained by three vortex identification methods, it is found that Ω_R and Liutex methods (third generation) are suitable for capturing the vortex structures in the large separated flow. Ω_R method is not sensitive with threshold and Liutex is a vector with being unique, accurate and Galilean invariant. In addition, the vortex structures are corresponding to the dominant positive/negative axial Liutex and a bound vortex pair. And the streamlines around the hull are spiral in the large separated flow, indicating that the flow in corresponding region is rotational.

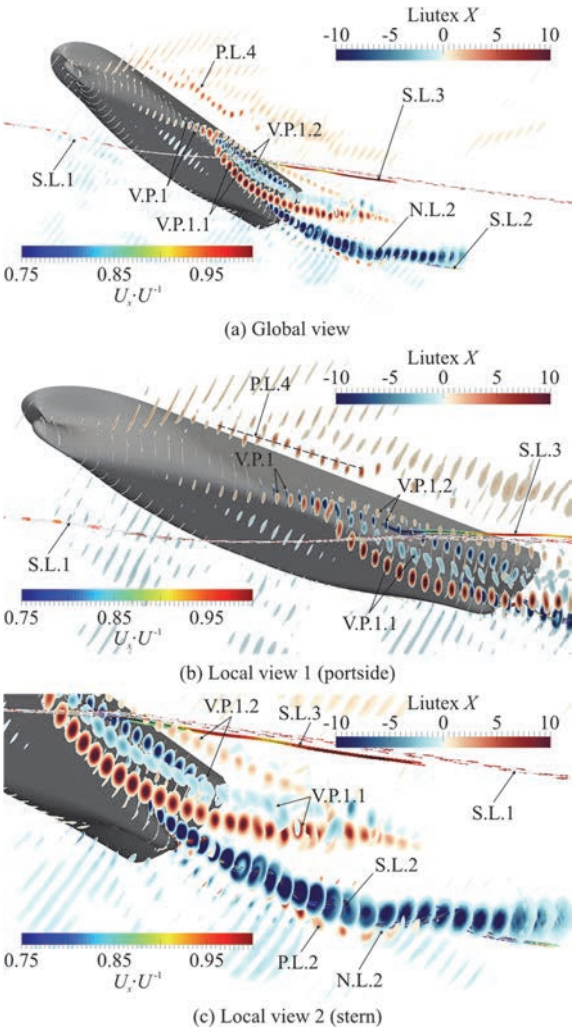

Fig. 10 (Color online) Evolution of axial Liutex and streamlines at $T+1/4T$

Although the flow field of PMM is further analyzed in this paper, the detail of local flow field is not fine enough. In the next work, the local fine flow around the hull will be the focus. In addition, the towing tests with large drift angle such as 40°, 60°, will also be studied.

References

[1] Simonsen C., Stern F. Flow pattern around an appended tanker hull form in simple maneuvering conditions [J]. *Computers and Fluids*, 2005, 34(2): 169-198.

[2] Xing T. BKW-RS-DES of unsteady vortical flow for KVLCC2 at large drift angle [C]. *International Conference on Numerical Ship Hydrodynamics*, Ann Arbor, Michigan, USA, 2007.

[3] Xing T., Carrica P., Stern F. Large-scale RANS and DDES computations of KVLCC2 at drift angle 0 degree [C]. *Gothenburg 2010: A Workshop on CFD in Ship Hydrodynamics*, Gothenburg, Sweden, 2010.

[4] Xing T., Bhushan S., Stern F. Vortical and turbulent structures for KVLCC2 at drift angle 0, 12, and 30 degrees [J]. *Ocean Engineering*. 2012, 55: 23-43.

[5] Ohashi K., Hino T. Flow comparisons of DES, DDES and URANS for a circular cylinder [J]. *Ship Technology Research*, 2009, 56(2): 87-92.

[6] Wang J., Ren Z., Wan D. Study of a container ship with breaking waves at high froude number using URANS and DDES methods [J]. *Journal of Ship Research*, 2020, 64(4): 346-356.

[7] Ren Z., Wang J., Wan D. Numerical simulation of ship bow wave breaking using DES and RANS [C]. *The 9th International Conference on Computational Methods* (ICCM2018), Rome, Italy, 2018, 1001-1012.

[8] Kandasamy M., Xing T., Stern F. Unsteady free surface wave-induced separation: Vortical structures and instabilities [J]. *Journal of Fluids and Structures*, 2009, 25(2): 343-363.

[9] Xing T., Kandasamy M., Stern F. Unsteady free-surface wave-induced separation: analysis of turbulent structures using detached eddy simulation and single-phase level set [J]. *Journal of Turbulence*, 2007, 8: N44.

[10] Pinto-Heredero A., Xing T., Stern F. URANS and DES analysis for a Wigley hull at extreme drift angles [J]. *Journal of Marine Science and Technology*, 2010, 15(4): 295-315.

[11] Bhushan S., Xing T., Stern F. Vortical structures and instability analysis for athena wetted transom flow with full-scale validation [J]. *Journal of Fluids Engineering*, 2012, 134(3): 031201.

[12] Heydari M., Sadat-Hosseini H. Analysis of propeller wake field and vortical structures using *k-ω* SST method [J]. *Ocean Engineering*, 2020, 204: 107247.

[13] Sakamoto N., Carrica P. M., Stern F. URANS simulations of static and dynamic maneuvering for surface combatant: Part 1. Verification and validation for forces, moment, and hydrodynamic derivatives [J]. *Journal of Marine Science and Technology*, 2012, 17(4): 422-445.

[14] Sakamoto N., Carrica P., Stern F. URANS simulations of static and dynamic maneuvering for surface combatant: Part 2. Analysis and validation for local flow characteristics [J]. *Journal of Marine Science and Technology*, 2012, 17(4): 446-468.

[15] Yoon H., Simonsen C., Benedetti L. et al. Benchmark CFD validation data for surface combatant 5415 in PMM maneuvers–Part I: Force/moment/motion measurements [J]. *Ocean Engineering*, 2015, 109: 705-734.

[16] Yoon H., Longo J., Toda Y. et al. Benchmark CFD validation data for surface combatant 5415 in PMM maneuvers–Part II: Phase-averaged stereoscopic PIV flow field measurements [J]. *Ocean Engineering*. 2015, 109: 735-750.

[17] Meng Q. J., Wan D. C. Numerical simulations of viscous flow around the obliquely towed KVLCC2M model in deep and shallow water [J]. *Journal of Hydrodynamics*, 2016, 28(3): 506-518.

[18] Ren Z., Wang J., Wan D. Investigation of the flow field of a ship in planar motion mechanism tests by the vortex identification method [J]. *Journal of Marine Science and Engineering*, 2020, 8(9): 649.

[19] Shen Z., Wan D., Carrica P. Dynamic overset grids in OpenFOAM with application to KCS self-propulsion and maneuvering [J]. *Ocean Engineering*, 2015, 108: 287-306.

[20] Wang J. H., Wan D. C. Numerical simulation of pure yaw motion using dynamic overset grid technology [J]. *Chinese Journal of Hydrodynamics*. 2016, 31(5): 567-574(in Chinese).

[21] Wang J., Zou L., Wan D. CFD simulations of free running ship under course keeping control [J]. *Ocean Engineering*, 2017, 141: 450-464.

[22] Berberović E., van Hinsberg N. P., Jakirlić S. et al. Drop impact onto a liquid layer of finite thickness: dynamics of the cavity evolution [J]. *Physical Review E*, 2009, 79(3): 036306.

[23] Menter F., Kuntz M., Langtry R. Ten years of industrial experience with the SST turbulence model [J]. *Turbulence, Heat and Mass Transfer*, 2003, 4(1): 625-632.

[24] Zhao W. W., Wan D. C. Detached-eddy simulation of flow past tandem cylinders [J]. *Applied Mathematics and Mechanics (English Edition)*, 2016, 37(12): 1272-1281.

[25] Zhao W., Zou L., Wan D. et al. Numerical investigation of vortex-induced motions of a paired-column semi-submersible in currents [J]. *Ocean Engineering*, 2018, 164: 272-283.

[26] Wang Y. Q., Gao Y. S., Xu H. et al. Liutex theoretical system and six core elements of vortex identification [J]. *Journal of Hydrodynamics*, 2020, 32(2): 197-211